

# Two-dimensional Electronic Spectroscopy Using Rotating Optical Flats

Patrick C. Tapping,<sup>†</sup> Yin Song,<sup>‡</sup> Yoichi Kobayashi,<sup>¶</sup> Gregory D. Scholes,<sup>§</sup> and Tak W. Kee<sup>\*,†</sup>

<sup>†</sup>*Department of Chemistry, The University of Adelaide, North Terrace, Adelaide, South Australia 5005, Australia*

<sup>‡</sup>*Department of Physics, University of Michigan, 450 Church Street, Ann Arbor, Michigan 48109, United States of America*

<sup>¶</sup>*Department of Applied Chemistry, College of Life Sciences, Ritsumeikan University, 1-1-1 Nojihigashi, Kusatsu, Shiga 525-8577, Japan*

<sup>§</sup>*Department of Chemistry, Princeton University, Washington Road, Princeton, New Jersey 08540, United States of America*

E-mail: tak.kee@adelaide.edu.au

Phone: +61-8-8313-5314

## Abstract

In two-dimensional electronic spectroscopy (2DES), precise control of the arrival time of ultrashort laser pulses is critical to correlating the molecular states that are accessed in the experiment. In this work, we demonstrate a 2D electronic spectrometer design with an interferometric phase stability of  $\sim\lambda/250$  at 600 nm. First, we present a new method for controlling pulse delay times based on transmission through pairs of optical flats rotated perpendicular to the beam propagation direction. Second, the calibration methods required to achieve adequate timing precision are also reported. Compared to existing designs using translating wedges, the rotating optical flats can achieve equivalent optical delay with a shorter path length in glass, reducing errors due to spectral dispersion of the broadband laser pulses used in 2DES. Our approach presents a simple, low-cost technique for multidimensional optical spectroscopy that is capable of resolving complex light-induced dynamics.

## Introduction

The use of two-dimensional (2D) spectroscopy in the visible region is a relatively recent development,<sup>1,2</sup> owing to the difficulty of maintaining high phase stability of the multiple laser pulses required in this spectral region. As an extension of pump-probe or transient absorption spectroscopy, 2D visible spectroscopy, or 2D electronic spectroscopy (2DES), can resolve electronic interactions and energy pathways in photoactive materials, thus has proven useful in a variety of fields such as organic or inorganic semiconductors and light-harvesting materials.<sup>3-12</sup> The mechanisms of photosynthesis have received particular attention,<sup>13-17</sup> where 2DES has revealed the presence of quantum coherences in biological systems and sparked debate over their role in the light-harvesting process.<sup>18-23</sup> A wide variety of spectrometer designs have been demonstrated, with several reviews in the literature describing the theory of operation and common layouts, including their strengths and weaknesses.<sup>2,24-31</sup> Spectral coverage across the visible range and into the ultraviolet has been demonstrated,<sup>32-34</sup> and the

technique extended to higher-order, multidimensional spectrometers.<sup>35–37</sup>

Fundamental to all designs is the generation of a Fourier transformed excitation axis, which is produced by the varied delay of a pair of laser excitation pulses with interferometric precision. A widely used delay scheme in 2DES involves transmission of laser beams through a pair of antiparallel glass wedges,<sup>25,38–42</sup> where translating one wedge varies the path length through glass. Another scheme that has been employed involves the use of a pulse shaper,<sup>33,34,39,43–46</sup> which offers convenience and rapid data acquisition through a programmable pulse sequence. Compared to pulse shapers, glass wedges offer a wider transmission bandwidth and a significantly lower cost of implementation. However, the transmitted beam exhibits a displacement after passing through a pair of glass wedges. As a result, the generated signal is misaligned relative to the reference beam, potentially decreasing the sensitivity of 2DES. This issue, however, is absent in spectrometers employing a pulse shaper. With drawbacks from the use of glass wedges and pulse shapers in 2DES, the development of an alternative approach that addresses these issues is desirable.

In this Article, we demonstrate a 2D electronic spectrometer that employs a delay technique using a pair of rotating optical flats (ROFs). The methods required to achieve the necessary interferometric precision and their implementation for 2DES are also reported. The ROFs provide comparable accuracy and delay range as wedges with the benefits of a shorter glass path length, reducing effects of spectral dispersion which can be severe with the broad bandwidth laser pulses used in 2DES. Additionally, the use of a pair of ROFs allows the laser pulse to be delayed precisely without any beam displacement. In contrast to the limitations of pulse shapers, ROFs offer transmission of a broad bandwidth and a low cost of implementation.

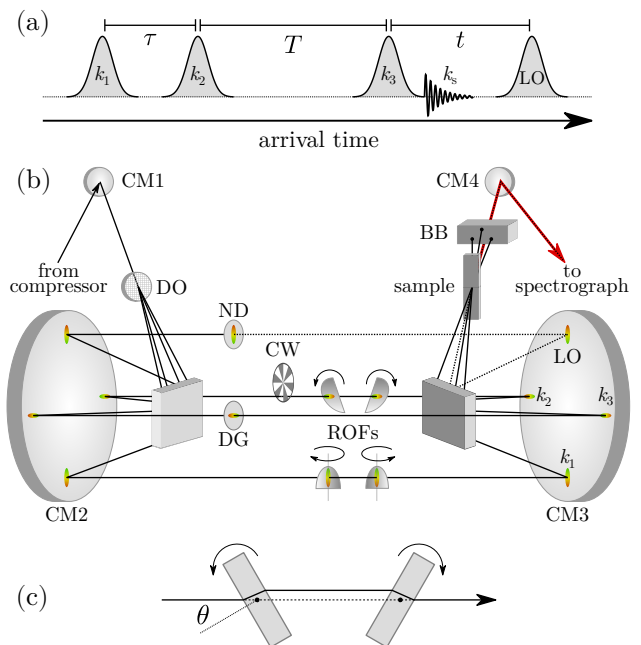


Figure 1: (a) Two delay stages control the arrival time of the  $\mathbf{k}_1$  and  $\mathbf{k}_2$  laser pulses relative to  $\mathbf{k}_3$  and the LO to create the required coherence ( $\tau$ ) and population ( $T$ ) times indicated. (b) Layout of the 2D spectrometer. CM: concave mirrors, DO: 2-dimensional diffractive optic, ND: neutral density filter, DG: delay glass, CW: chopper wheel, ROFs: rotating optical flats, BB: beam block. The positions of the laser pulses are labeled with  $\mathbf{k}_n$  and LO. The third-order signal (red line) is emitted from the sample on the same path as the LO (dotted line). (c) Beam path through a pair of ROFs, indicating the changed path length with no overall beam displacement.

## Methods

The pulse sequence for 2DES is depicted in Figure 1a. The delay between the first two pulses,  $\mathbf{k}_1$  and  $\mathbf{k}_2$ , defines the coherence time,  $\tau$ , while the delay between the second and third pulse,  $\mathbf{k}_3$ , is the population time,  $T$ .<sup>25</sup> The detected signal,  $\mathbf{k}_s$ , is emitted following the third pulse and is detected interferometrically with an attenuated local oscillator (LO) pulse separated by some time,  $t$ . The two phase matching conditions to produce a third-order signal are  $\mathbf{k}_s = -\mathbf{k}_1 + \mathbf{k}_2 + \mathbf{k}_3$  and  $\mathbf{k}_s = +\mathbf{k}_1 - \mathbf{k}_2 + \mathbf{k}_3$ , which are termed the rephasing and nonrephasing components, respectively.<sup>24,25,47</sup> In the box-

cars geometry (Figure 1b), the nonrephasing component is collected separately by swapping the roles of the  $\mathbf{k}_1$  and  $\mathbf{k}_2$  pulses (Figure 1a), in that  $\mathbf{k}_2$  arrives before  $\mathbf{k}_1$ .

Driving the spectrometer requires a suitable laser source with a spectrum that covers the region of interest for the target sample. Ideally, the source should be compressed to the transform limit to yield the highest time resolution for the experiment. In this work, the output of a regenerative amplifier (Spitfire Pro XP 100F, Spectra-Physics) provided 100 fs laser pulses centered at 800 nm with 1 kHz repetition rate. This output was directed to a home-built, 400 nm-pumped non-collinear optical parametric amplifier (NOPA) to produce a broadband output centered around 600 nm.<sup>48,49</sup> A single-grating and single-prism compressor compressed the pulses down to  $\sim 13$  fs,<sup>50–53</sup> as measured by frequency-resolved optical gating (FROG).<sup>54</sup> The NOPA spectrum and FROG traces are shown in the Supporting Information.

The spectrometer was based on a diffractive optic (DO) and boxcars layout, which is depicted in Figure 1b. The compressed laser pulse was focused on the DO (MS-203-Q-Y-A, Holo/Or) using a  $f = 500$  mm concave mirror (CM1). The four first-order beams generated by the DO were directed with a small steering mirror onto a  $f = 500$  mm concave mirror (CM2) which collimated the beams to form the box geometry. The locations of the excitation beams  $\mathbf{k}_1$ ,  $\mathbf{k}_2$ ,  $\mathbf{k}_3$ , and the local oscillator (LO) are shown in Figure 1b.  $\mathbf{k}_1$  and  $\mathbf{k}_2$  each passed through separate ROFs, which comprised a pair of fused-silica windows (226-1211M, Eksma Optics) with a thickness of  $\sim 0.8$  mm. Each pair was formed from a single window, cut in half to ensure the closest possible match in thickness and optical properties. Each window was mounted on a piezo rotation stage (CONEX-AG-PR100P, Newport), capable of  $0.001^\circ$  angle increments. Back reflections from the optical flat (OF) were used to align the windows and rotation stages so the rotational axis was perpendicular to the beam propagation. The rotational axis was also parallel to the direction of the beam spatial dispersion caused by the DO, as shown in Figure 1b, in order to optimize the

usable area of the OF once rotated. By rotating the OF pair in equal but opposite directions, delay was produced by changing the effective glass thickness and path length. However, overall the beam remained undeviated through the delay stage, as shown in Figure 1c.  $\mathbf{k}_3$  passed through a fixed delay glass (DG), chosen to approximately match the maximum possible delay available for  $\mathbf{k}_1$  and  $\mathbf{k}_2$ . The LO passed through a  $\sim 1$  mm thick neutral density (ND) filter to attenuate it by 4 orders of magnitude and an additional  $\sim 0.8$  mm OF to place it  $\sim 250$  fs after  $\mathbf{k}_3$ . The four beams were focused using a  $f = 300$  mm concave mirror (CM3) and steered onto the sample. A beam block (BB) masked all beams except the LO and the third-order signal emitted collinearly with the LO, which were collimated with a  $f = 300$  mm concave mirror (CM4) and directed to an imaging spectrograph and camera (Shamrock SR303-i and Newton 970, Andor). The camera acquired spectra at 500 Hz, synchronized to a mechanical chopper wheel (MC2000B, ThorLabs) positioned to modulate one of the excitation beams at 250 Hz. In this way, each spectrum from the camera consisted of light from two laser shots. True shot-to-shot acquisition would provide an incremental improvement in data quality,<sup>55</sup> but in this case the acquisition rate was limited by the speed of the camera. Consecutive pairs of spectra alternating between  $I_{\lambda,\text{on}}$  (signal + LO) and  $I_{\lambda,\text{off}}$  (LO only) were collected to give  $I_\lambda = (I_{\lambda,\text{on}} - I_{\lambda,\text{off}}) / I_{\lambda,\text{off}}$ . An acquisition for a given time ( $\tau, T$ ) contained 100 pairs of spectra, which were averaged to give the  $\Delta I / I$  signal in the 2DES spectrum.

The output from the compressor was horizontally polarized, which was maintained for all beams in the spectrometer, however insertion of  $\lambda/2$  plates in to the lines for polarization-sensitive experiments is possible provided the correct relative timings are preserved.<sup>56</sup> The pulse energy at the sample position was 15 nJ per excitation pulse with a full-width-at-half-maximum spot size of 25  $\mu\text{m}$ .

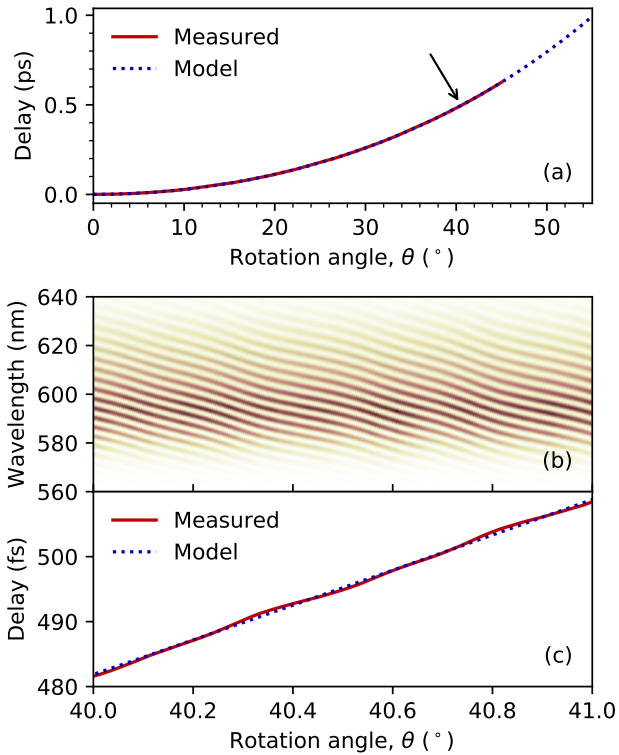


Figure 2: (a) Calibration curves for optical delay as a function of OF rotation angle using a theoretical model (dotted), or measured by spectral interferometry (solid). The arrow indicates the region magnified in the following panels. (b) Segment of the spectral interference pattern used to construct the measured calibration curve. (c) The measured calibration curve shows deviations from the model because of surface roughness or other imperfections in the OF.

## Results and Discussion

The relationship between the OF rotation angle and optical delay can be modeled to a first approximation by considering the changes in beam path through the OF and air, as shown in Figure 2a and detailed in the Supporting Information. The model was used to fit the data by varying the OF thickness and refractive index. An accuracy of  $\sim 1$  fs was achieved across the full OF rotation range. However, the accuracy of this model is insufficient for 2DES, which requires control of pulse arrival times to a sub-cycle precision, hence a more accurate method of delay calibration is required. To address this issue, we used a spectral interferom-

etry method inspired by techniques described previously,<sup>25,57,58</sup> and the results are shown in Figure 2. Using this method, the sample was replaced with a 50- $\mu\text{m}$  pinhole, the  $\mathbf{k}_2$  and LO beams were blocked, and scattered light in the signal direction from the  $\mathbf{k}_1$  and  $\mathbf{k}_3$  beams was captured by the spectrograph. The OF rotation angle,  $\theta$ , for the  $\mathbf{k}_1$  delay was stepped from  $0^\circ$  to  $45^\circ$  and the resulting interference pattern recorded, a segment of which is shown in Figure 2b. Because of the nonlinear relationship between  $\theta$  and delay time, a variable angle step was used, equivalent to approximately 0.1 fs intervals. The spectra were processed by a Fourier transform, Heaviside-like filter, and inverse Fourier transform, followed by unwrapping of the complex phase angle along the OF rotation angle axis.<sup>58</sup> The result is a measured delay time as a function of  $\theta$ , as shown in Figures 2a and c (solid red); the equivalent model-only curve is also shown for comparison (dotted blue). The calibration process was repeated for the second delay stage by stepping the  $\mathbf{k}_2$  delay with the  $\mathbf{k}_1$  beam blocked. Deviations from the model are clearly visible in Figure 2c as wavy curves. The obtained calibration curves were interpolated and used as delay-to-angle lookup tables by the spectrometer control software. We note that a calibration curve can be obtained for every pixel in the detection frequency axis, which may be used to study the extent of spectral dispersion caused by the changing OF path length as a function of delay time. This effect is discussed further below, with analysis found in the Supporting Information.

The importance of the delay calibration procedure is demonstrated in Figure 3. The data segments show spectral slices where  $\tau = 0$  fs, which require movement of the  $\mathbf{k}_1$  and  $\mathbf{k}_2$  relative to the  $\mathbf{k}_3$  pulse (Figure 1a) to yield  $T$  values ranging from 0 to 50 fs. This transient-grating experiment is highly sensitive to any spectrometer phase issues attributed to pulse timing errors. With given  $\tau$  and  $t$  values, a steady interference pattern should be produced, manifesting as straight horizontal lines (the intensity variations are due to the sample response from varying  $T$ ). The data collected using the model only (Figure 3a) exhibits severe deviations from

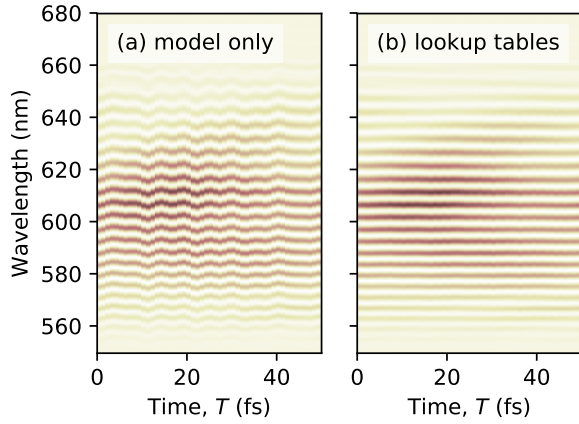


Figure 3: Comparison of raw data quality using (a) only the angle-to-delay model for the rotating OF pairs versus (b) calibrated lookup table built using spectral interferometry. Both plots show the same transient grating slice ( $\tau = 0$  fs), created by synchronous stepping of the  $\mathbf{k}_1$  and  $\mathbf{k}_2$  delay times. The idealized model is unable to account for OF imperfections, causing the wavy patterns due to delay timing mismatch.

straight lines, which are attributable to the mismatch of the  $\mathbf{k}_1$  and  $\mathbf{k}_2$  delays over this range, thus any 2D data collected under these conditions would be unreliable. In contrast, Figure 3b shows an identical segment of data, but using the delay-to-angle lookup tables. These data appear as a series of straight lines, indicating that the  $\mathbf{k}_1$  and  $\mathbf{k}_2$  delays are well matched. Re-calibration of the delays should only be required if the rotational stages or OFs are moved or realigned. The calibration of the delays is insensitive to changes to the NOPA spectrum or compressor, provided that the input alignment to the spectrometer is maintained. Stability and repeatability of the rotational stages and calibrations can be checked by performing a transient grating experiment such as those shown in Figure 3. Because this experiment depends on the precise, synchronous movement of both the  $\mathbf{k}_1$  and  $\mathbf{k}_2$  delay times (thus all four rotational stages), any errors in the calibration curves or drift in the rotational stage positioning can be observed clearly. We note that the transient grating data shown in Figure 3b were collected several weeks after the lookup tables

were generated, showing the stability of the calibration over this period. Furthermore, each set of collected 2D data contains a transient grating slice ( $\tau = 0$ ) which may be inspected to ensure validity of the calibration lookup tables.

The  $\mathbf{k}_1$ ,  $\mathbf{k}_2$  and  $\mathbf{k}_3$  were overlapped in time by performing a procedure analogous to a 2D FROG measurement conducted in the transient grating geometry.<sup>54</sup> Using a methanol sample with the LO blocked, the  $\mathbf{k}_1$  and  $\mathbf{k}_2$  delays were independently varied by approximately  $\pm 20$  fs around the arrival time of the  $\mathbf{k}_3$  pulse. The intensity of the signal as a function of the  $\mathbf{k}_1$  and  $\mathbf{k}_2$  delay times was fitted to a bivariate normal distribution to find the origin, where  $\tau = T = 0$  fs.

The passive phase stability afforded by the boxcars layout is demonstrated in Figure 4, where phase analysis as a function of acquisition time is shown. In this experiment, the interferogram from a cresyl violet (dye) sample was collected while  $\tau$  and  $T$  were fixed (Figure 4a). Variations in the measured interferogram are

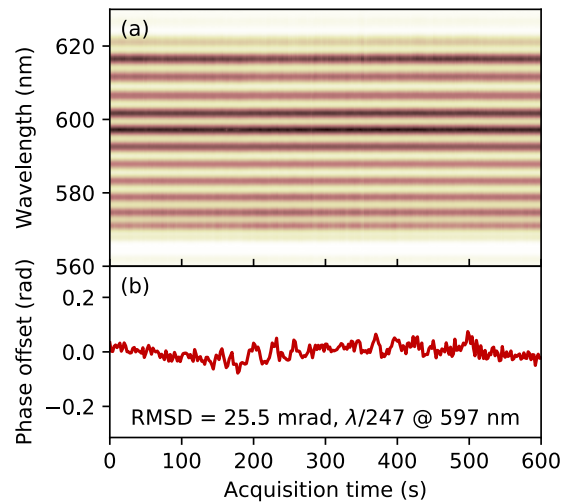


Figure 4: (a) Interference pattern and (b) computed phase stability of the spectrometer over a short time scale, approximating the duration of a single 2D scan (for a given population time,  $T$ ). Sample was a cresyl violet solution with delays fixed so that  $\tau = 0$  fs,  $T = 195$  fs and spectra acquired at 2 s intervals. The stability over a longer time scale is shown in the Supporting Information.

reflected as phase offsets, attributed to mis-

match of the  $\mathbf{k}_s$  and LO arrival times due to factors such as vibration, air turbulence and temperature changes, or through scattering from the sample. The measured phase stability at 597 nm was  $\lambda/247$  over 10 minutes (Figure 4b), which approximates the data acquisition time required for a single 2D spectrum for a given  $T$ . Over a longer period of 6 hours the phase stability was measured at  $\lambda/217$  (Supporting Information), comparable to or exceeding the specifications of some previously reported designs.<sup>33,38,42,58–62</sup>

In the experiment, data were collected by acquiring spectra while stepping the  $\mathbf{k}_1$  or  $\mathbf{k}_2$  delay over  $\tau$  to create the rephasing or non-rephasing components, respectively, for a given  $T$  (Figure 1a). The  $\mathbf{k}_1$  and  $\mathbf{k}_2$  delays were then moved by equal delay times to produce a new value of  $T$  and the process repeated. The raw data set is thus intensity as a function of detection wavelength at each  $\tau$  and  $T$  time,  $I(\lambda, \tau, T)$ . Typical values for  $\tau$  is 45 fs at 0.2 fs steps for both the rephasing and nonrephasing components of the 2D electronic spectrum. The upper limit of  $T$  is constrained by the achievable optical delay produced by the ROFs, which is approximately 600 fs at  $\theta = 45^\circ$  in this apparatus (Figure 2a). Beyond  $\theta = 45^\circ$ , the resolution of the rotation stages starts to decrease, where a  $0.001^\circ$  increment yields an optical delay of  $\sim 30$  as for a 0.85 mm thick glass. At  $\theta = 5^\circ$ , the accuracy of the delay is an order of magnitude higher than that.

Processing of the raw data to produce a 2D spectrum follows a similar procedure described by Anna et al.<sup>63,64</sup> The raw intensity data,  $I(\lambda, \tau, T)$ , is converted to separate rephasing and nonrephasing components in the frequency domain,  $I_R(f_3, f_1, T)$  and  $I_{NR}(f_3, f_1, T)$ , first by interpolating the detection wavelength,  $\lambda$ , to detection frequency,  $f_3$ , using significant oversampling ( $2^{12}$  or  $2^{13}$  points) to avoid peak shape distortions due to the nonlinear relationship.<sup>65</sup> An inverse Fourier transform along  $f_3$  reveals the detected signal appearing around time  $t$ . The LO and background noise components are removed while retaining the signal, which is Fourier transformed back to the frequency domain to give the signal spectrum. These spectra

are complex-valued, but the real and imaginary parts are identical apart from a  $\pi/2$  phase shift. A Fourier transform with respect to  $\tau$  gives the excitation frequency axis,  $f_1$ . During this step, edge-padding to the same dimensions as  $f_3$  may be used to smooth the peak shapes. Finally, the data are phased,<sup>2,24,64</sup> removing the linear spectral phase due to the signal–LO delay  $t$ , plus accounting for contributions from  $\mathbf{k}_1$  and  $\mathbf{k}_2$  timing errors. The final complex-valued spectra have the real or imaginary parts representing the absorptive or dispersive components of the sample, respectively. The complete procedure for phasing using the projection-slice theorem is detailed in the Supporting Information.

Figure 5 shows 2DES spectra at  $T = 110$  fs of cresyl violet perchlorate in methanol with an absorbance of  $\sim 0.5$  in a 1-mm path length cuvette. The 3 panels present the real parts of the (a) rephasing and (b) nonrephasing components, as well as their (c) sum total, which represents the absorptive spectrum. The dispersive spectrum is represented by the imaginary parts, which are shown in the Supporting Information. The elongated peak shape in Figure 5c is attributed to overlapping ground-state absorption around 590 nm and stimulated emission contributions at 610 nm and 625 nm. Oscillations of the peaks occur over  $T$  (see Supporting Information video) in both the rephasing and nonrephasing components, indicative of vibrational coherences and consistent with previous cresyl violet data in the literature.<sup>40,66,67</sup> Note that the laser spectrum used can have an influence on peak shapes,<sup>68</sup> in this case limiting the extent of the ground-state absorption feature into the high-energy region (Supporting Information).

The primary requirement for a multidimensional spectrometer design is achieving precise control of the laser pulse arrival times while maintaining the overall stability of the system. Vibration, air turbulence, and temperature fluctuations all have the possibility of perturbing the relative timings of the pulses, causing undesirable phase shifts. The phase shifts manifest as either noise or phantom signals, resulting in corrupted data. For example, with 600 nm light, data corruption can be caused by

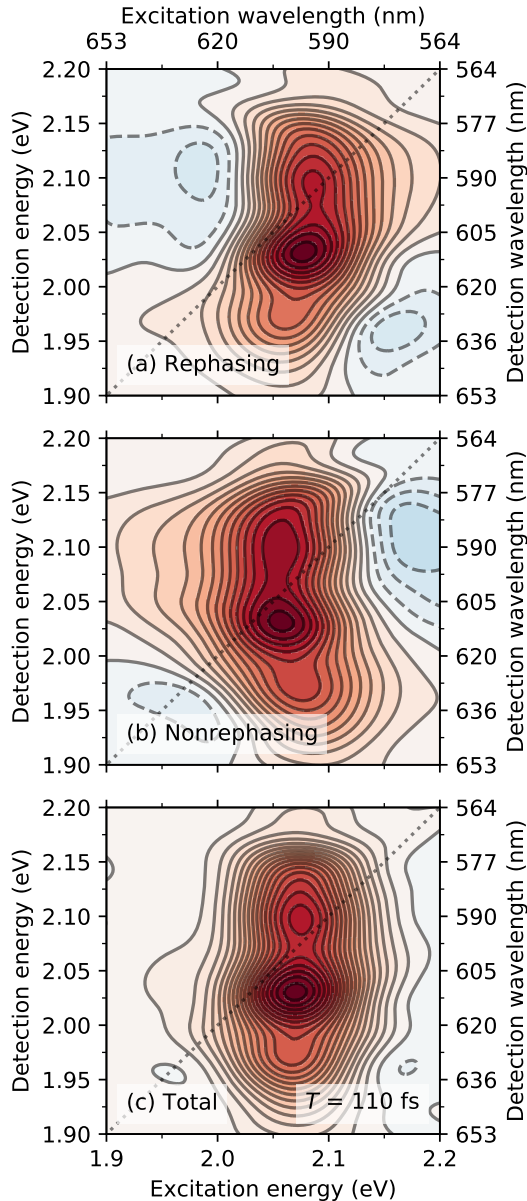


Figure 5: Real parts of the cresyl violet data at population time  $t = 110$  fs. The total absorptive spectrum (c) is the sum of the rephasing (a) and nonrephasing (b) components.

an error in relative pulse delays of 1 fs, equivalent to a full  $\pi$  phase inversion. Such an error may be caused by either movement of a mirror by merely 150 nm or by refractive index changes of air due to either temperature or turbulence. It is clear that a high phase stability is critical in the 2DES experiment.

Various spectrometer designs have been demonstrated and described in several reviews in the literature.<sup>28–30</sup> The two most common beam geometries are the boxcars type de-

scribed in this work, and the pump-probe type, where the first and second excitation pulses are collinear and the signal is emitted in the same direction as the third pulse, which also serves as the LO. The pump-probe geometry automatically provides purely absorptive spectra without the requirement of manual phasing but, as the first and second excitation pulses are indistinguishable, it cannot provide separated rephasing and nonrephasing components unless a phase cycling scheme is used.<sup>69,70</sup> Individual analysis of the rephasing and nonrephasing spectra can be valuable in some situations,<sup>27,40,56,71,72</sup> such as distinguishing electronic from vibrational coherences.<sup>40</sup>

Control of the pulse timings has been achieved in a number of ways. Translating mirrors were used in the initial designs,<sup>2</sup> which have the benefit of an all-reflective spectrometer, excluding spectral dispersion effects that are inherent in transmissive designs. This advantage is particularly important when ultrabroadband laser pulses are used. This approach is effective in producing the relatively coarse population time delays.<sup>39,46,73</sup> Sufficient, sub-fs precision required for coherence time delays can also be achieved with careful engineering,<sup>61,62</sup> but the total delay range is significantly limited. Alternatively, more complicated methods such as rotating reference frame acquisition are necessary to produce the required coherence time steps.<sup>66,74</sup> Transmissive delays using translating glass wedges are another common method,<sup>25,38–42</sup> where the optical path length is changed by modifying the effective glass thickness, as discussed further below. A similar design based on a Babinet-Soleil compensator uses birefringent wedges to produce a pair of collinear, variably delayed pulses suitable for excitation pulses in a pump-probe geometry.<sup>60,75</sup> Recently, femtosecond pulse shapers based on spatial light modulators or acousto-optic programmable dispersive filters have become more widespread.<sup>33,34,39,43–46</sup> These optical components have the advantage of easily producing reliable coherence times, and can be rapidly adjusted to allow phase cycling methods and minimize waiting time for mechanical delay positioning. Interestingly, despite these

advantages, a hybrid spectrometer that can use either translation stage or pulse shaper-based delays was recently described by Tollerud and Davis.<sup>29</sup> Their instrument exhibited several issues related to the pulse shaper under some conditions, particularly in the measurements with long coherence times. Transmissive delays using ROFs, to our knowledge, have been demonstrated only once before for use in 2DES.<sup>59</sup> However, the design differs from that described in this work due to the use of a single rotation stage and a folding mirror with two important consequences. First, the delay range was limited to 80 fs, suitable only for generating coherence time delays. Second, the use of folding mirrors introduces additional sources of phase instability.

The spectrometer detailed in this work is most closely related to designs using the box-cars layout and translating wedges to control pulse delays, thus it shares many of the same advantages and disadvantages.<sup>28,29</sup> The primary disadvantages are (1) the limited delay range required to sample long population times, (2) the relatively slow acquisition times due to waiting on delay stage positioning, and (3) the need for manual phasing of the processed data. The advantages include simplicity of design and intrinsic passive phase stability. In addition, the design presented here lowers the cost of a 2D electronic spectrometer by making use of the ROF delay stages. Compared to the cost of suitable linear translation stages with controller and wedged glass,<sup>40,64</sup> the rotation stages and OF are competitive, while a pulse-shaper based design is an order of magnitude more expensive.

While translating wedges and ROFs share many similarities, there are some key differences. Clearly, as seen in Figure 2a, there is a nonlinear relationship between  $\theta$  and the optical delay by the ROFs (Supporting Information), while the delay is linearly proportional to stage position for the translating wedges. The varying precision of the programmed delay over the range of rotation angles is a potential issue. The interplay of the OF thickness, rotation stage capabilities, plus required delay range and interval must be considered to ensure sufficient precision at the maximum delay

times where  $\theta$  is large. Transmission through the OFs also varies with angle, and depends on the polarization of the light. Using the horizontally polarized output of the compressor, the  $\mathbf{k}_1$  or  $\mathbf{k}_2$  beams are p- or s-polarized, respectively, relative to their ROFs (Figure 1b), and transmission through the OF pairs is described by the Fresnel equations,<sup>76</sup> as shown in the Supporting Information. The linear response of the pump-probe experiment allows simple correction of the data using the predicted intensity change of the pump with OF rotation angle. Interestingly, because of the opposing effects of the p- and s-polarized beams, the intensity of the third-order signal of the 2D data only changes by 5% for OF rotation angles up to 40°, and is negligible below  $\sim 30^\circ$  (Supporting Information). Despite commercially available OF possessing better surface flatness and smoothness specifications than wedges, significant delay deviations from the expected model are still observed during calibration (Figure 2c). These imperfections are not isolated to ROFs. Significant errors in wedge based delays attributed to surface roughness was reported by Augulis and Zigmantas,<sup>57</sup> where a displacement-to-delay lookup table scheme was suggested as a means to overcome these defects. Wedge calibration issues were further discussed more recently by Bolzonello et al.,<sup>41</sup> whose use of 4° CaF<sub>2</sub> wedges required a more careful scheme for determination of the calibration factors. However, despite a rigorous multi-step calibration process, imperfections in the wedges still induced phase deviations which required correction during data processing. Zhu et al. also investigated the suitability of single-parameter wedge calibration factors considering the influence of flatness and surface roughness, and discussed peak shifts or distortions which might result from calibration errors.<sup>58</sup> Imperfect optics are not only a problem limited to transmissive delays; Zheng et al. also showed that the phase stability of an all-reflective interferometric delay design was limited by surface flatness of the mirrors used.<sup>61</sup> We suggest that the lookup table calibration method used in this work may improve any mechanically-based delay system by correcting for arbitrary system-

atic imperfections in either optics or hardware, potentially leading to improved data quality and allowing the use of low-cost motion control devices.

Spectral dispersion, or pulse chirping, is a consideration for any transmission-based delay system due to the broad spectral bandwidth used for 2DES. Insertion of varying amounts of dispersive material necessarily results in deviations from the ideal, transform-limited pulse shape across the delay range. Brixner et al. calculated a pulse broadening factor of  $1.6 \times 10^{-4}$  for their 40 fs pulse duration with  $T = 300$  fs and the use of fused silica wedges.<sup>25</sup> After correcting for this dispersion they showed that it made negligible impact on the resulting spectral shapes, a conclusion shared by other groups using translating-wedge delays.<sup>38,58</sup> However, with increasing laser pulse bandwidth and longer induced delays the dispersion effect can become significant, requiring either correction during the data processing stage,<sup>41</sup> or the use of all-reflective delay mechanisms.<sup>61,62,67</sup> Interestingly, the ROFs outperform translating wedges in terms of spectral dispersion. Although a positive optical delay is achieved by increasing the optical path length through glass and decreasing that through air, there is a notable difference in the two approaches. Because the ROFs produce a beam displacement between the OF pair, the reduction of path length through air is less than the increase in path length of glass (note the absence of beam displacement after passing through the pair). Consequently, when compared to translating wedges, the same induced delay requires a smaller increase in path through glass, hence reducing the beam path through glass by up to 40%. This effect is particularly significant with broadband ultrashort pulses such as the ones used in this work. Further details and calculations are shown in the Supporting Information. The reduced spectral dispersion also has an effect on the error of delay time. The spectral interferometry method used to construct the delay lookup tables (Figure 2) produces a calibration curve for each detection wavelength, thus the effect of varying spectral dispersion with delay time can be directly measured. We found a  $\pm 0.1\%$  difference

in delay time across the spectral range used in this experiment (Supporting Information), which is approximately half the error in the translating-wedge calibration factors measured by Zhu et al.<sup>58</sup> The increased performance of the ROF-based design is consistent with the smaller change in glass path length required for the same optical delay time, as calculated in the Supporting Information.

In the boxcars geometry, positioning of the four beams is crucial to obtain the correct phase matching conditions for the heterodyne signal detection. Transmission through pairs of wedges necessarily produces a permanent beam displacement (Supporting Information). This effect can be minimized by having a small wedge angle and ensuring the separation between the pair is as short as practicable. Displacement after passing through a typical  $1^\circ$  fused silica wedge pair separated by a few mm can be expected to be  $< 0.1$  mm, but is linearly dependent on both cut angle and separation (Supporting Information). For this reason, the use of wedges with larger angles to increase delay range can introduce significant issues, as beam displacement will change the vector of the emitted signal,  $\mathbf{k}_s$ , so that it is no longer collinear with the LO, reducing the quality of the obtained interferogram. For example, with a wedge angle of  $4^\circ$  and a separation of 10 mm, the beam displacement is estimated to be close to 10% of the beam diameter of  $\sim 3$  mm. With this level of beam displacement, the spatial mismatch between  $\mathbf{k}_s$  and the LO can cause the interferometric signal intensity to decrease by 10% (Supporting Information).

Finally, we note that the spectrometer presented in this work is a simple design for demonstrating the use of ROFs to produce pulse delays suitable for multidimensional spectroscopy. With additional hardware, improvements such as dual-modulation may be made,<sup>41,42,62,66,67,77</sup> which can reduce the influence of beam scattering and potentially collect pump-probe data in the same experiment. Rotating reference frame heterodyne detection may also be used to reduce the number of acquisitions required in the  $\tau$  axis and decrease total acquisition time, but it requires control of the LO arrival time

which may be implemented with additional delay stages.<sup>66,74</sup> Increasing the achievable population time is also desirable, and is in-principle a straightforward task. The delay produced by the ROFs is directly proportional to the OF thickness, but increasing the delay range in this way comes at the cost of a decreased resolution. With the rotation stages used in this work, we expect a population time delay of 1 ps to be achievable using  $\sim 1.5$ -mm thick OFs while still maintaining sufficient coherence time accuracy. Alternatively, a conventional translating-mirror delay stage may be installed to selectively delay  $\mathbf{k}_3$  and the LO relative to  $\mathbf{k}_1$  and  $\mathbf{k}_2$ , eliminating a pair of ROFs. However, this approach involves breaking of the boxcars layout and rebalancing the relative pulse delays, thus care must be taken when reassembling the boxcars geometry to ensure accurate re-imaging of the beam pattern at the sample position. The delay range offered by the ROFs in this work is suitable for the study of systems with fast dynamics, such as electron or metal-metal charge transfer,<sup>3,4,78</sup> as well as many molecular systems.<sup>8,19–21</sup> However, an extended delay range may be required for systems with long coherence times or where low frequency vibrational or phonon modes are of interest.<sup>5,41</sup> If a conventional delay stage is installed to control the population times, and the ROFs are only required to produce the relatively short coherence time delays, the issue of slow acquisition rate could also be addressed. The rotation stages used in this work have the advantages of providing the requisite accuracy over a large rotation angle, but are slow to position. Galvanometer-type actuators are fast to position and can offer the required resolution, but only operate over a relatively small angle (and thus delay) range. Using custom built driver circuitry to synchronize the galvanometer positioning with the camera frame rate, fast acquisition techniques could be employed<sup>55</sup> without requiring additional tracer beams or electronics.<sup>79</sup>

## Conclusions

In conclusion, we have presented a new method to use ROFs to produce optical delays with interferometric precision suitable for use in multidimensional electronic spectroscopy. When compared to translating wedge designs, the ROFs offer a low-cost solution with reduced effects from spectral dispersion due to varying glass thickness. We have demonstrated the successful acquisition of 2D spectra of cresyl violet using a spectrometer based on a pair of ROF delay lines.

**Acknowledgement** PCT, TWK and GDS acknowledge the Australian Research Council for funding support (LE0989747 and DP160103797).

## Supporting Information Available

Characterization of laser pulse and spectrometer stability, phasing of 2D data, influence of laser spectrum on peak shape, full 2D data, rotating glass delay model, spectral dispersion and beam displacement compared to translating wedges.

## References

- (1) Hybl, J. D.; Albrecht, A. W.; Faeder, S. M. G.; Jonas, D. M. Two-dimensional Electronic Spectroscopy. *Chem. Phys. Lett.* **1998**, *297*, 307–313.
- (2) Hybl, J. D.; Albrecht Ferro, A.; Jonas, D. M. Two-dimensional Fourier Transform Electronic Spectroscopy. *J. Chem. Phys.* **2001**, *115*, 6606–6622.
- (3) Song, Y.; Clifton, S. N.; Pensack, R. D.; Kee, T. W.; Scholes, G. D. Vibrational Coherence Probes the Mechanism of Ultrafast Electron Transfer in Polymer-Fullerene Blends. *Nat. Commun.* **2014**, *5*, 4933.

- (4) De Sio, A.; Troiani, F.; Maiuri, M.; Réhault, J.; Sommer, E.; Lim, J.; Huelga, S. F.; Plenio, M. B.; Rozzi, C. A.; Cerullo, G. et al. Tracking the Coherent Generation of Polaron Pairs in Conjugated Polymers. *Nat. Commun.* **2016**, *7*, 13742.
- (5) Bakulin, A. A.; Morgan, S. E.; Kehoe, T. B.; Wilson, M. W. B.; Chin, A. W.; Zigmantas, D.; Egorova, D.; Rao, A. Real-Time Observation of Multiexcitonic States in Ultrafast Singlet Fission Using Coherent 2D Electronic Spectroscopy. *Nat. Chem.* **2016**, *8*, 16–23.
- (6) Mandal, A.; Chen, M.; Foszycz, E. D.; Schultz, J. D.; Kearns, N. M.; Young, R. M.; Zanni, M. T.; Wasielewski, M. R. Two-dimensional Electronic Spectroscopy Reveals Excitation Energy-dependent State Mixing during Singlet Fission in a Terrylenedimide Dimer. *J. Am. Chem. Soc.* **2018**, *140*, 17907–17914.
- (7) Borca, C. N.; Zhang, T.; Li, X.; Cundiff, S. T. Optical Two-dimensional Fourier Transform Spectroscopy of Semiconductors. *Chem. Phys. Lett.* **2005**, *416*, 311–315.
- (8) Kobayashi, Y.; Chuang, C.-H.; Burda, C.; Scholes, G. D. Exploring Ultrafast Electronic Processes of Quasi-type II Nanocrystals by Two-dimensional Electronic Spectroscopy. *J. Phys. Chem. C* **2014**, *118*, 16255–16263.
- (9) Seiler, H.; Palato, S.; Sonnichsen, C.; Baker, H.; Kambhampati, P. Seeing Multiexcitons through Sample Inhomogeneity: Band-edge Biexciton Structure in CdSe Nanocrystals Revealed by Two-dimensional Electronic Spectroscopy. *Nano Lett.* **2018**, *18*, 2999–3006.
- (10) Lim, J.; Paleček, D.; Caycedo-Soler, F.; Lincoln, C. N.; Prior, J.; von Berlepsch, H.; Huelga, S. F.; Plenio, M. B.; Zigmantas, D.; Hauer, J. Vibronic Origin of Long-lived Coherence in an Artificial Molecular Light Harvester. *Nat. Commun.* **2015**, *6*, 7755.
- (11) Lee, Y.; Das, S.; Malamakal, R. M.; Meloni, S.; Chenoweth, D. M.; Anna, J. M. Ultrafast Solvation Dynamics and Vibrational Coherences of Halogenated Boron-dipyrromethene Derivatives Revealed through Two-dimensional Electronic Spectroscopy. *J. Am. Chem. Soc.* **2017**, *139*, 14733–14742.
- (12) Otto, J. P.; Wang, L.; Pochorovski, I.; Blau, S.; Aspuru-Guzik, A.; Bao, Z.; Engel, G. S.; Chiu, M. Disentanglement of Excited-state Dynamics with Implications for FRET Measurements: Two-dimensional Electronic Spectroscopy of a BODIPY-functionalized Cavitand. *Chem. Sci.* **2018**, *9*, 3694–3703.
- (13) Brixner, T.; Stenger, J.; Vaswani, H. M.; Cho, M.; Blankenship, R. E.; Fleming, G. R. Two-dimensional Spectroscopy of Electronic Couplings in Photosynthesis. *Nature* **2005**, *434*, 625–628.
- (14) Zigmantas, D.; Read, E. L.; Mančal, T.; Brixner, T.; Gardiner, A. T.; Cogdell, R. J.; Fleming, G. R. Two-dimensional Electronic Spectroscopy of the B800–B820 Light-harvesting Complex. *Proc. Natl. Acad. Sci. USA* **2006**, *103*, 12672–12677.
- (15) Dostál, J.; Pšenčík, J.; Zigmantas, D. In Situ Mapping of the Energy Flow through the Entire Photosynthetic Apparatus. *Nat. Chem.* **2016**, *8*, 705.
- (16) Akhtar, P.; Zhang, C.; Do, T. N.; Garab, G.; Lambrev, P. H.; Tan, H.-S. Two-dimensional Spectroscopy of Chlorophyll a Excited-state Equilibration in Light-harvesting Complex II. *J. Phys. Chem. Lett.* **2017**, *8*, 257–263.
- (17) Lambrev, P. H.; Akhtar, P.; Tan, H.-S. Insights into the Mechanisms and Dynamics of Energy Transfer in Plant

- Light-harvesting Complexes from Two-dimensional Electronic Spectroscopy. *Biochim. Biophys. Acta, Bioenergetics* **2019**, DOI: 10.1016/j.bbabi.2019.07.005.
- (18) Engel, G. S.; Calhoun, T. R.; Read, E. L.; Ahn, T.-K.; Mančal, T.; Cheng, Y.-C.; Blankenship, R. E.; Fleming, G. R. Evidence for Wavelike Energy Transfer through Quantum Coherence in Photosynthetic Systems. *Nature* **2007**, *446*, 782–786.
- (19) Collini, E.; Wong, C. Y.; Wilk, K. E.; Curmi, P. M. G.; Brumer, P.; Scholes, G. D. Coherently Wired Light-harvesting in Photosynthetic Marine Algae at Ambient Temperature. *Nature* **2010**, *463*, 644–647.
- (20) Jun, S.; Yang, C.; Isaji, M.; Tamaki, H.; Kim, J.; Ihee, H. Coherent Oscillations in Chlorosome Elucidated by Two-dimensional Electronic Spectroscopy. *J. Phys. Chem. Lett.* **2014**, *5*, 1386–1392.
- (21) Halpin, A.; Johnson, P. J. M.; Tempelaar, R.; Murphy, R. S.; Knoester, J.; Jansen, T. L. C.; Miller, R. J. D. Two-dimensional Spectroscopy of a Molecular Dimer Unveils the Effects of Vibronic Coupling on Exciton Coherences. *Nat. Chem.* **2014**, *6*, 196.
- (22) Duan, H.-G.; Prokhorenko, V. I.; Cogdell, R. J.; Ashraf, K.; Stevens, A. L.; Thorwart, M.; Miller, R. J. D. Nature Does Not Rely on Long-lived Electronic Quantum Coherence for Photosynthetic Energy Transfer. *Proc. Natl. Acad. Sci. USA* **2017**, *114*, 8493–8498.
- (23) Wang, L.; Allodi, M. A.; Engel, G. S. Quantum Coherences Reveal Excited-state Dynamics in Biophysical Systems. *Nat. Rev. Chem.* **2019**, *3*, 477–490.
- (24) Jonas, D. M. Two-dimensional Femtosecond Spectroscopy. *Annu. Rev. Phys. Chem.* **2003**, *54*, 425–463.
- (25) Brixner, T.; Mančal, T.; Stiopkin, I. V.; Fleming, G. R. Phase-stabilized Two-dimensional Electronic Spectroscopy. *J. Chem. Phys.* **2004**, *121*, 4221–4236.
- (26) Hochstrasser, R. M. Two-dimensional Spectroscopy at Infrared and Optical Frequencies. *Proc. Natl. Acad. Sci. USA* **2007**, *104*, 14190–14196.
- (27) Brańczyk, A. M.; Turner, D. B.; Scholes, G. D. Crossing Disciplines — A View on Two-dimensional Optical Spectroscopy. *Ann. Phys.* **2014**, *526*, 31–49.
- (28) Fuller, F. D.; Ogilvie, J. P. Experimental Implementations of Two-dimensional Fourier Transform Electronic Spectroscopy. *Annu. Rev. Phys. Chem.* **2015**, *66*, 667–690.
- (29) Tollerud, J. O.; Davis, J. A. Coherent Multi-dimensional Spectroscopy: Experimental Considerations, Direct Comparisons and New Capabilities. *Prog. Quantum Electron.* **2017**, *55*, 1–34.
- (30) Oliver, T. A. A. Recent Advances in Multidimensional Ultrafast Spectroscopy. *R. Soc. Open Sci.* **2018**, *5*, 171425.
- (31) Gelzinis, A.; Augulis, R.; Butkus, V.; Robert, B.; Valkunas, L. Two-dimensional Spectroscopy for Non-specialists. *Biochim. Biophys. Acta, Bioenergetics* **2019**, *1860*, 271–285.
- (32) West, B. A.; Moran, A. M. Two-dimensional Electronic Spectroscopy in the Ultraviolet Wavelength Range. *J. Phys. Chem. Lett.* **2012**, *3*, 2575–2581.
- (33) Krebs, N.; Pugliesi, I.; Hauer, J.; Riedle, E. Two-dimensional Fourier Transform Spectroscopy in the Ultraviolet with Sub-20 fs Pump Pulses and 250–720 nm Supercontinuum Probe. *New J. Phys.* **2013**, *15*, 085016.
- (34) Song, Y.; Konar, A.; Sechrist, R.; Roy, V. P.; Duan, R.; Dziurgot, J.; Policht, V.; Matutes, Y. A.;

- Kubarych, K. J.; Ogilvie, J. P. Multi-spectral Multidimensional Spectrometer Spanning the Ultraviolet to the Mid-infrared. *Rev. Sci. Instrum.* **2019**, *90*, 013108.
- (35) Turner, D. B.; Nelson, K. A. Coherent Measurements of High-order Electronic Correlations in Quantum Wells. *Nature* **2010**, *466*, 1089–1092.
- (36) Zhang, Z.; Wells, K. L.; Tan, H.-S. Purely Absorptive Fifth-order Three-dimensional Electronic Spectroscopy. *Opt. Lett.* **2012**, *37*, 5058–5060.
- (37) Zhang, Z.; Wells, K. L.; Seidel, M. T.; Tan, H.-S. Fifth-order Three-dimensional Electronic Spectroscopy Using a Pump-probe Configuration. *J. Phys. Chem. B* **2013**, *117*, 15369–15385.
- (38) Nemeth, A.; Sperling, J.; Hauer, J.; Kauffmann, H. F.; Milota, F. Compact Phase-stable Design for Single- and Double-quantum Two-dimensional Electronic Spectroscopy. *Opt. Lett.* **2009**, *34*, 3301–3303.
- (39) Schlau-Cohen, G. S.; Ishizaki, A.; Fleming, G. R. Two-dimensional Electronic Spectroscopy and Photosynthesis: Fundamentals and Applications to Photosynthetic Light-harvesting. *Chem. Phys.* **2011**, *386*, 1–22.
- (40) Turner, D. B.; Wilk, K. E.; Curmi, P. M. G.; Scholes, G. D. Comparison of Electronic and Vibrational Coherence Measured by Two-dimensional Electronic Spectroscopy. *J. Phys. Chem. Lett.* **2011**, *2*, 1904–1911.
- (41) Bolzonello, L.; Volpato, A.; Meneghin, E.; Collini, E. Versatile Setup for High-quality Rephasing, Non-rephasing, and Double Quantum 2D Electronic Spectroscopy. *J. Opt. Soc. Am. B* **2017**, *34*, 1223–1233.
- (42) Oblinsky, D. G.; Ostroumov, E. E.; Scholes, G. D. Drop-in Two-dimensional Electronic Spectroscopy Based on Dual Modulation in the Pump-probe Geometry. *Opt. Lett.* **2019**, *44*, 2653–2656.
- (43) Turner, D. B.; Stone, K. W.; Gundogdu, K.; Nelson, K. A. Invited Article: The Coherent Optical Laser Beam Recombination Technique (COLBERT) Spectrometer: Coherent Multidimensional Spectroscopy Made Easier. *Rev. Sci. Instrum.* **2011**, *82*, 081301.
- (44) Tyagi, P.; Saari, J. I.; Walsh, B.; Kabir, A.; Crozatier, V.; Forget, N.; Kambhampati, P. Two-color Two-dimensional Electronic Spectroscopy Using Dual Acousto-optic Pulse Shapers for Complete Amplitude, Phase, and Polarization Control of Femtosecond Laser Pulses. *J. Phys. Chem. A* **2013**, *117*, 6264–6269.
- (45) Tollerud, J. O.; Hall, C. R.; Davis, J. A. Isolating Quantum Coherence Using Coherent Multi-dimensional Spectroscopy with Spectrally Shaped Pulses. *Opt. Express* **2014**, *22*, 6719–6733.
- (46) Kearns, N. M.; Mehlenbacher, R. D.; Jones, A. C.; Zanni, M. T. Broadband 2D Electronic Spectrometer Using White Light and Pulse Shaping: Noise and Signal Evaluation at 1 and 100 kHz. *Opt. Express* **2017**, *25*, 7869–7883.
- (47) Cho, M. Coherent Two-Dimensional Optical Spectroscopy. *Chem. Rev.* **2008**, *108*, 1331–1418.
- (48) Wilhelm, T.; Piel, J.; Riedle, E. Sub-20-fs Pulses Tunable across the Visible from a Blue-pumped Single-pass Noncollinear Parametric Converter. *Opt. Lett.* **1997**, *22*, 1494–1496.
- (49) Shirakawa, A.; Kobayashi, T. Non-collinearly Phase-matched Femtosecond Optical Parametric Amplification with a 2000  $\text{cm}^{-1}$  Bandwidth. *Appl. Phys. Lett.* **1998**, *72*, 147–149.

- (50) Lai, M.; Lai, S. T.; Swinger, C. Single-grating Laser Pulse Stretcher and Compressor. *Appl. Opt.* **1994**, *33*, 6985–6987.
- (51) Akturk, S.; Gu, X.; Kimmel, M.; Trebino, R. Extremely Simple Single-prism Ultrashort-pulse Compressor. *Opt. Express* **2006**, *14*, 10101–10108.
- (52) Fork, R. L.; Cruz, C. H. B.; Becker, P. C.; Shank, C. V. Compression of Optical Pulses to Six Femtoseconds by Using Cubic Phase Compensation. *Opt. Lett.* **1987**, *12*, 483–485.
- (53) Chauhan, V.; Bowlan, P.; Cohen, J.; Trebino, R. Single-diffraction-grating and Grism Pulse Compressors. *J. Opt. Soc. Am. B* **2010**, *27*, 619–624.
- (54) Trebino, R.; DeLong, K. W.; Fittinghoff, D. N.; Sweetser, J. N.; Krumbügel, M. A.; Richman, B. A.; Kane, D. J. Measuring Ultrashort Laser Pulses in the Time-frequency Domain Using Frequency-resolved Optical Gating. *Rev. Sci. Instrum.* **1997**, *68*, 3277–3295.
- (55) Brazard, J.; Bizimana, L. A.; Turner, D. B. Accurate Convergence of Transient-absorption Spectra Using Pulsed Lasers. *Rev. Sci. Instrum.* **2015**, *86*, 053106.
- (56) Schlau-Cohen, G. S.; Dawlaty, J. M.; Fleming, G. R. Ultrafast Multidimensional Spectroscopy: Principles and Applications to Photosynthetic Systems. *IEEE J. Sel. Top. Quantum Electron.* **2012**, *18*, 283–295.
- (57) Augulis, R.; Zigmantas, D. Detector and Dispersive Delay Calibration Issues in Broadband 2D Electronic Spectroscopy. *J. Opt. Soc. Am. B* **2013**, *30*, 1770–1774.
- (58) Zhu, R.; Yue, S.; Li, H.; Leng, X.; Wang, Z.; Chen, H.; Weng, Y. Correction of Spectral Distortion in Two-dimensional Electronic Spectroscopy Arising from the Wedge-based Delay Line. *Opt. Express* **2019**, *27*, 15474–15484.
- (59) Cowan, M.; Ogilvie, J.; Miller, R. Two-dimensional Spectroscopy Using Diffractive Optics Based Phased-locked Photon Echoes. *Chem. Phys. Lett.* **2004**, *386*, 184–189.
- (60) Brida, D.; Manzoni, C.; Cerullo, G. Phase-locked Pulses for Two-dimensional Spectroscopy by a Birefringent Delay Line. *Opt. Lett.* **2012**, *37*, 3027–3029.
- (61) Zheng, H.; Caram, J. R.; Dahlberg, P. D.; Rolczynski, B. S.; Viswanathan, S.; Dolzhenkov, D. S.; Khadivi, A.; Talapin, D. V.; Engel, G. S. Dispersion-free Continuum Two-dimensional Electronic Spectrometer. *Appl. Opt.* **2014**, *53*, 1909–1917.
- (62) Son, M.; Mosquera-Vázquez, S.; Schlau-Cohen, G. S. Ultrabroadband 2D Electronic Spectroscopy with High-speed, Shot-to-shot Detection. *Opt. Express* **2017**, *25*, 18950–18962.
- (63) Anna, J. M.; Ostroumov, E. E.; Maghlaoui, K.; Barber, J.; Scholes, G. D. Two-dimensional Electronic Spectroscopy Reveals Ultrafast Downhill Energy Transfer in Photosystem I Trimers of the Cyanobacterium *Thermosynechococcus Elongatus*. *J. Phys. Chem. Lett.* **2012**, *3*, 3677–3684.
- (64) Anna, J. M.; Song, Y.; Dinshaw, R.; Scholes, G. D. Two-dimensional Electronic Spectroscopy for Mapping Molecular Photophysics. *Pure Appl. Chem.* **2013**, *85*, 1307.
- (65) Dorrer, C.; Belabas, N.; Likforman, J.-P.; Joffre, M. Spectral Resolution and Sampling Issues in Fourier-transform Spectral Interferometry. *J. Opt. Soc. Am. B* **2000**, *17*, 1795–1802.
- (66) Heisler, I. A.; Moca, R.; Camargo, F. V. A.; Meech, S. R. Two-dimensional Electronic Spectroscopy Based on Conventional Optics and Fast Dual Chopper Data Acquisition. *Rev. Sci. Instrum.* **2014**, *85*, 063103.

- (67) Ma, X.; Dostál, J.; Brixner, T. Broadband 7-fs Diffractive-optic-based 2D Electronic Spectroscopy Using Hollow-core Fiber Compression. *Opt. Express* **2016**, *24*, 20781–20791.
- (68) Nowakowski, P. J.; Khyasudeen, M. F.; Tan, H.-S. The Effect of Laser Pulse Bandwidth on the Measurement of the Frequency Fluctuation Correlation Functions in 2D Electronic Spectroscopy. *Chem. Phys.* **2018**, *515*, 214–220.
- (69) Tian, P.; Keusters, D.; Suzuki, Y.; Warren, W. S. Femtosecond Phase-coherent Two-dimensional Spectroscopy. *Science* **2003**, *300*, 1553–1555.
- (70) Myers, J. A.; Lewis, K. L. M.; Tekavec, P. F.; Ogilvie, J. P. Two-color Two-dimensional Fourier Transform Electronic Spectroscopy with a Pulse-shaper. *Opt. Express* **2008**, *16*, 17420–17428.
- (71) Cheng, Y.-C.; Fleming, G. R. Coherence Quantum Beats in Two-dimensional Electronic Spectroscopy. *J. Phys. Chem. A* **2008**, *112*, 4254–4260.
- (72) Volpato, A.; Bolzonello, L.; Meneghin, E.; Collini, E. Global Analysis of Coherence and Population Dynamics in 2D Electronic Spectroscopy. *Opt. Express* **2016**, *24*, 24773–24785.
- (73) Harel, E.; Fidler, A. F.; Engel, G. S. Single-shot Gradient-assisted Photon Echo Electronic Spectroscopy. *J. Phys. Chem. A* **2011**, *115*, 3787–3796.
- (74) Kramer, P. L.; Giammanco, C. H.; Tamimi, A.; Hoffman, D. J.; Sokolowsky, K. P.; Fayer, M. D. Quasi-rotating Frame: Accurate Line Shape Determination with Increased Efficiency in Noncollinear 2d Optical Spectroscopy. *J. Opt. Soc. Am. B* **2016**, *33*, 1143–1156.
- (75) Kearns, N.; Jones, A. C.; Kunz, M. B.; Allen, R. T.; Flach, J. T.; Zanni, M. T. Two-dimensional White-light Spectroscopy Using Supercontinuum from an All-normal Dispersion Photonic Crystal Fiber Pumped by a 70 MHz Yb Fiber Oscillator. *J. Phys. Chem. A* **2019**, *123*, 3046–3055.
- (76) Born, M.; Wolf, E.; Bhatia, A. B.; Clemmow, P. C.; Gabor, D.; Stokes, A. R.; Taylor, A. M.; Wayman, P. A.; Wilcock, W. L. *Principles of Optics: Electromagnetic Theory of Propagation, Interference and Diffraction of Light*, 7th ed.; Cambridge University Press, 1999.
- (77) Augulis, R.; Zigmantas, D. Two-dimensional Electronic Spectroscopy with Double Modulation Lock-in Detection: Enhancement of Sensitivity and Noise Resistance. *Opt. Express* **2011**, *19*, 13126–13133.
- (78) Kambhampati, P.; Son, D. H.; Kee, T. W.; Barbara, P. F. Solvent Effects on Vibrational Coherence and Ultrafast Reaction Dynamics in the Multicolor Pump-Probe Spectroscopy of Intervalence Electron Transfer. *J. Phys. Chem. A* **2000**, *104*, 10637–10644.
- (79) Fox, Z. W.; Blair, T. J.; Weakly, R. B.; Courtney, T. L.; Khalil, M. Implementation of Continuous Fast Scanning Detection in Femtosecond Fourier-transform Two-dimensional Vibrational-electronic Spectroscopy to Decrease Data Acquisition Time. *Rev. Sci. Instrum.* **2018**, *89*, 113104.

# Graphical TOC Entry

